Fermi-surface topology of $YBa_2Cu_3O_x$ with varied oxygen stoichiometry: A photoemission study

Rong Liu, B. W. Veal, A. P. Paulikas, J. W. Downey, P. J. Kostić, S. Fleshler, and U. Welp
Materials Science Division, Argonne National Laboratory, Argonne, Illinois 60439

C. G. Olson and X. Wu
Ames Laboratory and Department of Physics, Iowa State University, Ames, Iowa 50011

A. J. Arko and J. J. Joyce
Los Alamos National Laboratory, Los Alamos, New Mexico 87545
(Received 7 May 1992)

High-resolution angle-resolved photoemission measurements are reported for $YBa_2Cu_3O_x$ when oxygen stoichiometry x was varied between 6.3 and 6.9. Fermi surfaces were measured and their dependence on oxygen stoichiometry was monitored by observing the dispersing behavior of spectral features, scanning the entire first Brillouin zone. For $x=6.9$, measured Fermi surfaces correspond very well with the plane-related Fermi surfaces calculated from band theory. Relatively small changes in Fermi surfaces were observed when oxygen stoiochiometry was varied in the range $6.5 \leq x \leq 6.9$, where the material is metallic. However, significant changes in the spectral behavior were observed when the material becomes insulating.

I. INTRODUCTION

In the study of high-T_c copper oxide superconductors, an understanding of the normal-state properties has generally been regarded as key to understanding the superconductivity. For the normal state, the central issue has been whether a Fermi-liquid description is valid or not. Anomalous behavior in the normal state has been identified in various experiments, suggesting non-Fermi-liquid character.[1] On the other hand, Fermi surfaces (FS's) were clearly observed in $Bi_2Sr_2CaCu_2O_8$ (Refs. 2 and 3) and $YBa_2Cu_3O_{6.9}$ (Refs. 4–7) by angle-resolved photoelectron spectroscopy (ARPES). In addition, observations of FS's were also reported for $YBa_2Cu_3O_{6.9}$ using positron annihilation[8,9] and de Haas–van Alphen techniques.[10,11] Generally, good correspondence was found between the measured FS's and the FS's predicted by band theory.[12–15] However, many other theoretical models have also been proposed to describe these materials.[16–19] To date, no general agreement has been reached on what theoretical framework provides the best description.[20]

An apparently general property of the high-T_c oxides is that electrical conductivities can be readily controlled by varying the carrier concentration. This is accomplished with ion substitution, oxygen stoichiometry variation, or controlled state of order. For the $YBa_2Cu_3O_x$ system, T_c monotonically decreases from 92 to 0 K as oxygen stoichiometry x is varied from 6.9 to 6.4. Superconductivity is lost at the metal-insulator transition, which occurs near $x=6.4$. Thus a range of behavior, from metallic to insulating, can be systematically examined. This variability provides us with a rich parameter space in which to explore these materials.

A unique structural feature of $YBa_2Cu_3O_x$ is the presence of quasi-one-dimensional CuO chains in addition to CuO_2 planes which are common to all of the high-T_c copper oxides. With the chains fully occupied, at $x=7$, the material defines the ideal orthorhombic (ortho I) phase. As oxygen is removed from this structure, oxygen vacancies appear in the chains, while the planes remain relatively intact.[21] For oxygen-deficient material, there is a strong tendency for the vacancies to order.[22–24] Apparently, this ordering affects the carrier concentration and consequently T_c.[25,26] A dominant ordered form is the double-cell orthorhombic (ortho II) phase, which is characterized by alternately filled and empty chains in the chain basal plane. At $x=6$, the chains completely disappear since all oxygen is removed from the chain basal plane.

In this paper we report an ARPES study of the FS's of $YBa_2Cu_3O_x$ when oxygen stoichiometry is varied in the range $6.3 \leq x \leq 6.9$. We have acquired an extensive set of ARPES measurements at three oxygen stoichiometries in order to obtain a detailed mapping of the FS's and to study their dependence on oxygen content. We report measurements for the stoichiometries, $x \approx 6.9$, 6.5, and 6.3, which include, respectively, a 92-K superconductor in the ortho I structure, an approximately 50-K superconductor in the ortho II structure, and an insulating sample with stoichiometry very close to the metal-insulator transition. We have reported more limited studies of the FS and its variation with oxygen stoichiometry in earlier publications.[27,28]

Recently, Tobin *et al.*[6] reported an extensive ARPES study of untwinned fully oxygenated $YBa_2Cu_3O_{6.9}$. Those results provide a very useful reference work for the present study, in which oxygen content is varied. Of par-

ticular importance is the reported variation of spectral intensity with photon energy. In the present study, we have chosen to use those photon energies where spectral features are most intense and $h\nu=21.2$ eV (coincident with the energy of He I radiation). For the purpose of consistency and convenience of comparison, we have also performed measurements on $x=6.9$ samples. The acute features observed by Tobin *et al.*,[6] both near E_F and about 1 eV below E_F, were also observed in our twinned samples. For the $x=6.5$ stoichiometry, spectra were taken from both heavily twinned and from nearly twin-free samples.

In the remaining text of this paper, we will present, in separate sections, results for each of the three oxygen stoichiometries: $x=6.9$, 6.5, and 6.3. In Sec. III A we discuss the ARPES data measured on a $x=6.9$ sample taken at numerous **k** points in the first Brillouin zone (BZ). We discuss how the FS's were determined. The measured FS's are compared with the predictions of local-density-approximation (LDA) calculations and other model theories. In Sec. III B we compare the spectra measured on $x=6.5$ samples with those on $x=6.9$ samples at equivalent **k** points. We discuss the results with consideration for structural variations associated with changes in oxygen content. For $x=6.5$, ARPES data are compared to results of LDA calculations for the ortho II structure. In Sec. III C measurements on insulating $x\approx 6.3$ samples are presented and compared with those from metallic samples. We point out the fundamental spectral changes that occur at the onset of the metal-insulator transition.

II. EXPERIMENTAL DETAILS

The ARPES data were taken on single crystals of $YBa_2Cu_3O_x$, with typical dimensions $1\times1\times0.1$ mm^3 grown in gold crucibles using a self-flux technique.[29] To obtain oxygen stoichiometry $x\geq 6.9$, samples were heat treated in O_2 for 6 days at 480 °C followed by a 4-day treatment at 420 °C and a furnace cool to room temperature. Oxygen stoichiometries $x<6.9$ were normally fixed by quenching from 520 °C after equilibrating (for at least 48 h) in a controlled oxygen-nitrogen atmosphere.[25] After quenching (to liquid nitrogen), samples were aged at room temperature for at least 1 week to achieve a stable vacancy-ordered condition.[25] Superconducting transition temperatures were measured, on warming, in a 0.5-Oe field after cooling in zero field, with a superconducting quantum interference device (SQUID) magnetometer.[30] For the $x=6.9$ samples, T_c's were approximately 92 K; at $x=6.5$, T_c's were about 50 K. Transition widths were less than 2 K. One $x=6.5$ sample was detwinned by cooling it from 425 °C under uniaxial stress.[31] The stoichiometry was then reduced to $x=6.5$ by a heat treatment of 10 days duration at 450 °C in a sealed quartz tube containing about 1 g of ceramic $x=6.5$ sample. The ceramic acts as a buffer to fix the stoichiometry of the small (<1 mg) single crystal. The crystal remained nearly twin free after the heat treatment. Other crystals in this study were twinned.

ARPES measurements were made on the Ames-Montana ERG-Seya beam line[32] at the Synchrotron Radiation Center at Stoughton, Wisconsin, using the Seya monochromator with photon energies in the 15–30-eV range. Photoelectrons were energy analyzed using a 50-mm-radius hemispherical analyzer mounted on a goniometer. The analyzer has two degrees of rotational freedom. The angular resolution of the analyzer is 2° (full apex angle of acceptance cone), which corresponds to a **k** resolution of 0.073 Å^{-1} (about $\frac{1}{11}$ of the Γ-to-X distance in **k** space) for $h\nu=21.2$ eV. Numerous spectra were acquired using $h\nu=21.2$ eV radiation and a 5-eV pass energy for the electron analyzer. This photon energy was used so that comparison could be made with data collected by utilizing He I radiation. With these measurement conditions, the total-energy resolution (electron and photon) ΔE was 55 meV. Additional high-energy-resolution data ($\Delta E=20$–30 meV) were taken along symmetry lines, using $h\nu=21.2$, 17, and 28 eV, and a 2-eV pass energy for the analyzer. The position of the Fermi level was determined by measuring the Fermi edge of a clean platinum foil which was in electrical contact with the $YBa_2Cu_3O_x$ samples.

Before mounting in the sample chamber, sample orientations were determined by Laue x-ray diffraction. Mounted samples were cleaved *in situ* in a vacuum better than 4×10^{-11} Torr with the sample temperature at about 20 K.[33] The cleaved surfaces contain the *a-b* plane. The samples were mounted with the *c* and *a* (*b*) axes in the horizontal plane. After cleaving, the alignment of the surface normal was confirmed (or adjusted slightly, as needed) using ARPES spectra. The normal was readily obtained by monitoring the position and symmetry of the highly dispersive feature at about 1.5 eV binding energy that appears with high intensity at the $\bar{\Gamma}$ point when using $h\nu=24$ eV.[28] The photon beam from the monochromator was in the horizontal plane, striking the sample at an angle of approximately 40° from the surface normal; the beam was almost completely linearly polarized with the electric vector in the horizontal plane.

When twinned samples are used, $\bar{\Gamma}$-$\bar{Y}$ and $\bar{\Gamma}$-$\bar{X}$ are, of course, indistinguishable in ARPES since both *a* and *b* directions are probed simultaneously. Thus measurements taken at different electron-emission angles, acquired when the analyzer's vertical position (ϕ angle) or horizontal position (θ angle) is held fixed at 0°, corresponds to **k** vectors measured along the superimposed $\bar{\Gamma}$-$\bar{Y}$($\bar{X}$) symmetry lines in the BZ. However, because polarized light was used, a measurement acquired with the analyzer set at a horizontal position ($\theta=\theta_0$, $\phi=0$) is not equivalent to a measurement taken with the analyzer set at an equivalent vertical position ($\theta=0$, $\phi=\theta_0$). At equivalent binding energies, spectral weights for the complementary emission angles will differ.

ARPES measurements were made with the sample temperatures maintained at about 20 K. Unlike $Bi_2Sr_2CaCu_2O_8$, where a superconducting gap was observed when the sample was cooled below T_c,[34–36] no significant difference was observed in the photoemission spectra of $YBa_2Cu_3O_{6.9}$ when data were taken above and below T_c.[6,27] Therefore the spectra measured at 20 K,

even for samples with $T_c = 92$ and 50 K, are considered to represent properties of the normal state.

III. RESULTS

A. $YBa_2Cu_3O_{6.9}$

In angle-resolved photoemission, an energy distribution curve (EDC) is obtained by analyzing the energies of the photoelectrons emitted from a crystal surface in a well-defined emission angle while the incident-photon energy is held constant. In the photoemission process, the component of electron momentum parallel to the crystal surface ($\mathbf{k}_\parallel$) is conserved upon escaping from the solid. In the simple case of a two-dimensional crystal, the electron state is completely determined by $\mathbf{k}_\parallel$. Thus, by monitoring the dispersion of a spectral feature in the EDC as a function of emission angle, the energy-versus-momentum dispersion of a two-dimensional electron state can be mapped. A point on the FS is defined as a value of $\mathbf{k}$ at which a peak disperses across the Fermi level. In practice, a dispersing spectral feature is identified in a series of EDC's for a set of $\mathbf{k}$ points along some direction in $\mathbf{k}$ space. As the dispersing feature passes through E_F, an abrupt dropoff in spectral intensity occurs since photoemission only measures occupied electron states. Thus, to determine a point on the FS, we look for the combination of a dispersing spectral feature that signals an energy band moving toward E_F, followed by an abrupt intensity falloff as the spectral feature (energy band) passes through the Fermi level. Also, EDC's with a sharp Fermi-edge cutoff indicate that a band (or bands) lies at, or very close to, the Fermi level.

In general, accuracy of the FS measurements from ARPES is limited by errors in crystal alignment (estimated to be $\pm 1°$) and by the finite angular resolution of the detector (in our experiments, $\pm 1°$). Also, we note that it is relatively easier to locate the $\mathbf{k}$ value of a Fermi-level crossing when a peak has large dispersion. (The dispersing feature points toward the Fermi-level crossing.) If a peak is very close to E_F and shows little dispersion, then the error in the FS measurement might be relatively large. The difficulty is that the observed peak shape is determined by the spectral function in the sampled energy and momentum window convoluted by the Fermi and instrument functions. Thus one cannot determine, by inspection of one spectrum, if a peak near E_F results from a band lying entirely below E_F or from a band which overlaps E_F within the (energy and momentum) measurement window. One must look for abrupt changes in spectral intensity, as $\mathbf{k}$ is varied, to determine the FS. We also note that because of matrix elements and polarization selection rules, it is common for photoemission to fail to "see" a feature. On the other hand, if a distinct feature is observed, it is almost certain that the feature contains information about the occupied electronic structure of the material. A thorough investigation of the FS would require measurements along different directions in the BZ, using different photon energies as well as different symmetry configurations with respect to photon polarization, in order to obtain redundancy in the FS measurements.

As noted above, band mapping by ARPES is straightforward only for two-dimensional systems. $YBa_2Cu_3O_x$ appears to be sufficiently two dimensional so that variations in k_z may, to good approximation, be ignored. This approximation is supported by results of band calculations where it was shown that the electronic structure of $YBa_2Cu_3O_7$ has a rather small dispersion along k_z in most regions of the BZ.[12–15] We note that the typical $\mathbf{k}$ resolution (0.08 Å^{-1}) of our instruments is about $\frac{1}{3}$ of the Γ-to-Z distance in the BZ of $YBa_2Cu_3O_{7-\delta}$, in contrast to about $\frac{1}{10}$ of the Γ-to-X or the Γ-to-Y distance. Consequently, in studying in-plane dispersion, a significant fraction of the Γ-to-Z distance is routinely probed. In this paper we make the two-dimensional approximation and use the notations $\bar{\Gamma}$, $\bar{X}$, $\bar{Y}$, and $\bar{S}$ to designate symmetry points in the two-dimensional BZ.

Shown in Fig. 1 are the EDC's measured on a $x = 6.9$ sample using $h\nu = 21.2$ eV, with $\mathbf{k}$ scanning along (a) $\bar{\Gamma}$-$\bar{S}$ and (b) $\bar{\Gamma}$-$\bar{Y}(\bar{X})$ symmetry lines, respectively. The spectra are normalized to photon flux. The photoelectron-emission angles relative to the surface normal (θ and ϕ) are marked next to each curve. The $\mathbf{k}$ points, corresponding to each of the measured EDC's, are shown in the insets as open and solid circles in the BZ section. [Since this sample was twinned, $\mathbf{k}$ points are marked along both $\bar{\Gamma}$-$\bar{Y}$ and $\bar{\Gamma}$-$\bar{X}$ in the inset of Fig. 1(b)]. The value of $\mathbf{k}$ for a given θ and ϕ was obtained from

$$\mathbf{k}_\parallel = 0.514\ \text{Å}^{-1}\sqrt{E_{\text{kin}}}\,(\sin\theta\,\hat{\mathbf{x}} + \sin\phi\,\hat{\mathbf{y}})\ ,$$

where E_{kin} is the kinetic energy in eV, $\mathbf{k}_\parallel$ is the component of electron momentum parallel to the sample surface, and $\hat{\mathbf{x}}$ and $\hat{\mathbf{y}}$ are the unit vectors along the $\bar{\Gamma}$-$\bar{X}$ and $\bar{\Gamma}$-$\bar{Y}$ directions, respectively.

Figure 1 shows that, along both the $\bar{\Gamma}$-$\bar{S}$ and $\bar{\Gamma}$-$\bar{Y}(\bar{X})$

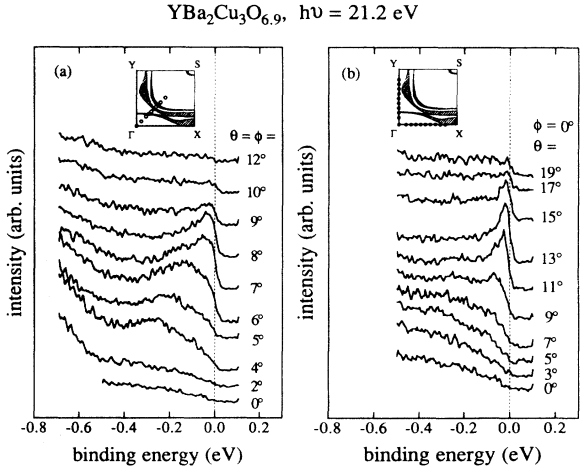

FIG. 1. Energy distribution curves (EDC's) measured on a $x = 6.9$ sample using $h\nu = 21.2$ eV, for $\mathbf{k}$ points along (a) $\bar{\Gamma}$-$\bar{S}$ and (b) $\bar{\Gamma}$-$\bar{Y}(\bar{X})$. The photoelectron-emission angles relative to the surface normal (θ and ϕ) are marked next to each curve. The corresponding $\mathbf{k}$ points are marked as open and solid circles in the Brillouin zone in the insets, along with the calculated Fermi surfaces (shaded regions) of Ref. 15. The solid circles indicate Fermi-level crossings observed in the spectra.

directions, when the analyzer is moved away from normal emission ($\bar{\Gamma}$ point), spectral features develop and disperse toward the Fermi level. Along $\bar{\Gamma}$-$\bar{S}$, we identify two bands that disperse through the Fermi level. A prominent feature first appears with high intensity at about 0.25 eV binding energy when $\theta=\phi=4°$ and crosses the Fermi level at about $\theta=\phi=9°$. The spectral intensity abruptly falls off as this band crosses E_F. Another feature, which appears as a shoulder at lower binding energies (most apparent when $\theta=\phi=6°$), also disperses across E_F. This feature is not well resolved because of its relatively low intensity and proximity to the neighboring peak. While it is not obvious at which **k** point this feature crosses E_F, we argue that the crossing occurs near $\theta=\phi=7°$. We observe that, at $\theta=\phi=7°$, the spectrum has a sharp Fermi edge, indicating that the low-binding-energy peak is cut off by the Fermi-Dirac function; however, the spectrum is still quite broad because of the near proximity of the neighboring peak at higher binding energy. At the next **k** point, $\theta=\phi=8°$, the spectrum also has a sharp Fermi edge, but a significantly narrower spectral feature now appears near E_F. This suggests that the band responsible for the first (low-binding-energy) peak has dispersed through E_F and the higher-binding-energy peak is now very close to E_F. We emphasize, however, that while the band crossing at $\theta=\phi=9°$ is quite clear (and closely agrees with the interpretation of Mante *et al.*[7]), the Fermi-level crossing assigned to the shoulder feature (at $\theta=\phi=7°$) is much more subjective. Mante *et al.* have also noted the presence of the shoulder, but do not assign a Fermi-level crossing.

The values of **k** for these two Fermi-level crossings (points on the FS) are indicated as solid circles on the BZ section in the inset of Fig. 1(a). Also shown in the inset are the calculated FS's projected along the k_z direction (shaded regions).[15] This presentation of the FS's (Ref. 15) reflects the amount of k_z dispersion in various regions of the BZ. For those FS's where the shaded regions are relatively narrow, the k_z dispersion is negligible and the two-dimensional approximation is well justified. We compare our measured FS's with this presentation, since in the ARPES measurements, information is integrated over a substantial fraction of the BZ length along k_z. Also, the value of k_z is not determined in ARPES. As seen in the inset, the two observed Fermi-level crossings are consistent with the two calculated FS's associated

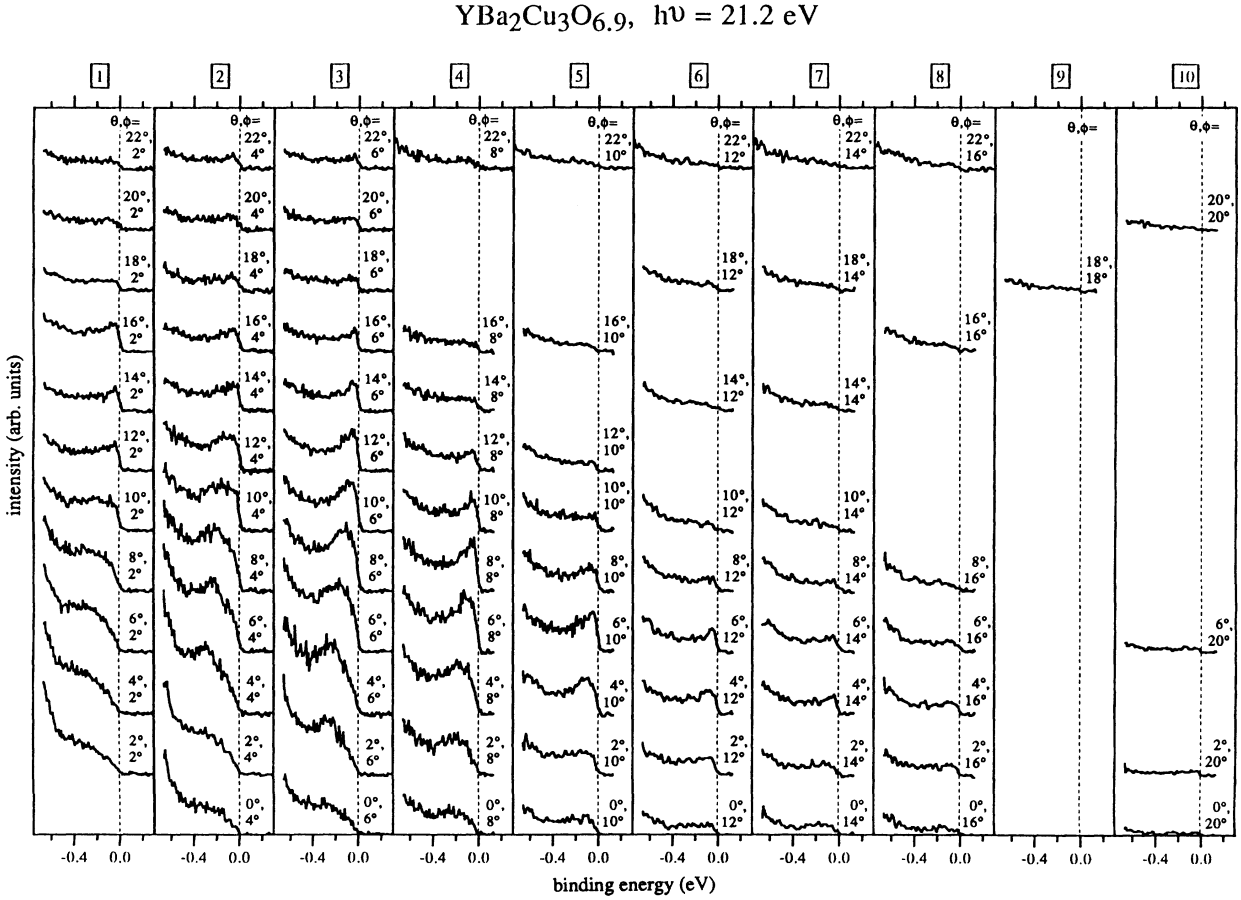

FIG. 2. EDC's measured on a $x=6.9$ sample using $h\nu=21.2$ eV. The photoelectron-emission angles relative to the surface normal (θ and ϕ) are marked next to each curve. Each vertical column of EDC's was measured with the ϕ angle held constant; thus, the corresponding **k** points fall on a line parallel to $\bar{\Gamma}$-$\bar{Y}(\bar{X})$ in the Brillouin zone shown in Fig. 3. All the spectra are normalized to the photon flux and are displayed on the same horizontal and vertical scales, but zeros are offset for clarity.

with the plane bands. Along $\bar{\Gamma}$-$\bar{Y}(\bar{X})$, a fairly narrow peak disperses through E_F at about $\theta=15°$ [solid circles in the inset of Fig. 1(b)].

Having examined the spectra along the $\bar{\Gamma}$-$\bar{S}$ and $\bar{\Gamma}$-$\bar{Y}(\bar{X})$ symmetry lines, we now consider the spectra for **k** in general regions of the BZ. Shown in Fig. 2 are the EDC's when **k** was scanned on a grid of points which encompasses the first BZ. The photoelectron-emission angles relative to the surface normal (θ and ϕ) are marked next to each curve. Throughout most of the zone, EDC's were measured in 2° increments in both θ and ϕ. Each vertical column of EDC's was measured with the ϕ angle held constant; thus, the corresponding **k** points fall on a line parallel to $\bar{\Gamma}$-$\bar{Y}(\bar{X})$ in the BZ shown in Fig. 3. In Fig. 3 we draw grids (dotted lines) for the k_x and k_y axes. The separation of the grid lines corresponds to 2° (for $h\nu=21.2$ eV) in θ and ϕ; thus, the value of **k** for each EDC in Fig. 2 can be easily located in the BZ shown in Fig. 3. These EDC's were measured using $h\nu=21.2$ eV and a 5-eV pass energy for the electron analyzer ($\Delta E=55$ meV). All the spectra are normalized to the photon flux. The spectra are displayed on the same horizontal and vertical scales, but zeros are offset for clarity.

We observe, in Fig. 2, that the spectral weights near E_F vary significantly throughout the first BZ. Spectral features with strong dispersing character appear with high intensity in approximately one quadrant of the zone (containing $\bar{\Gamma}$). The variation of the spectral intensity might be a result of matrix-element effects.

With this display, dispersing behavior along lines parallel to $\bar{\Gamma}$-$\bar{Y}(\bar{X})$ can be examined. In column 4, for example, spectral dispersion and an abrupt intensity falloff near ($\theta=10°$, $\phi=8°$) clearly signals a Fermi-level crossing (plotted as an open circle in Fig. 3). Similarly, in column 1, an abrupt intensity falloff near ($\theta=16°$, $\phi=2°$) indicates that a (relatively nondispersing) band has passed through

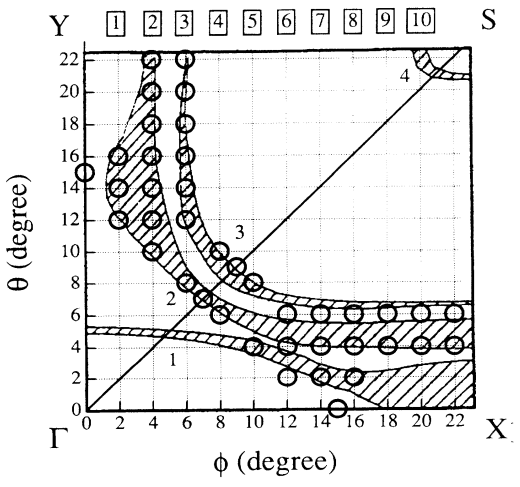

FIG. 3. Comparison of the measured Fermi surfaces of $YBa_2Cu_3O_{6.9}$ (open circles) determined from EDC measurements using $h\nu=21.2$ eV and the calculated Fermi surfaces of $YBa_2Cu_3O_7$ (shaded regions) of Ref. 15. Since the data were taken on twinned crystals, the Fermi-surface measurements were determined for half of the zone (the triangle section left of the $\bar{\Gamma}$-$\bar{S}$ line) and mapped into the other half by symmetry.

E_F. While many of the band crossings are clearly discernible in Fig. 2, we find, nonetheless, that the FS determination is substantially aided by examining band dispersion in different directions.

In Figs. 4(a)–4(d), we show EDC's along the $\bar{\Gamma}$-$\bar{S}$ line and along lines parallel to $\bar{\Gamma}$-$\bar{S}$. As usual, **k** points corresponding to the displayed EDC's appear as solid circles in the insets. It is clear that there are bands that pass through E_F along all these directions. As discussed above, shoulders on the lower-binding-energy side are apparent in some of the spectra, indicating that another nearly parallel band also disperses through E_F, forming the outer circle of the plane-related FS.

For **k** in the region near the $\bar{Y}(\bar{X})$ point (e.g., the upper portions of the columns 2 and 3 in Fig. 2), the spectra exhibit a low-intensity peak close to E_F that is relatively nondispersing. Under these circumstances (as discussed above), it is not clear whether the peak crosses E_F. In Figs. 5(a) and 5(b), we display the EDC's for **k** along different directions. Results are shown for two horizontal lines where the angle θ was held at constant at 22° and 16°, respectively. In Fig. 5(a) it is clear that at ($\theta=22°$, $\phi=4°$) and ($\theta=22°$, $\phi=6°$) a peak is observed close to, or at, E_F. Similarly, in Fig. 5(b), bands cross or lie in very close proximity to E_F at ($\theta=16°$, $\phi=2°$), ($\theta=16°$, $\phi=4°$), and ($\theta=16°$, $\phi=6°$).

Using these procedures to analyze EDC's taken at $h\nu=21.2$ eV (Figs. 1 and 2), we determined the FS's in the entire first BZ. The resulting FS's are shown as open circles in Fig. 3. Since the measurements were made on twinned crystals, signals from two almost orthogonal domains were superimposed. Consequently, we chose to determine FS's in one-half of the zone (the triangle section left of the $\bar{\Gamma}$-$\bar{S}$ line); results were then plotted to the other half symmetrically about the $\bar{\Gamma}$-$\bar{S}$ line. (Symmetry about the $\bar{\Gamma}$-$\bar{S}$ line can be observed in the spectra.)

Also shown in Fig. 3 are the calculated FS's projected along the k_z direction (shaded regions),[15] as described previously. We observe in Fig. 3 that the measured FS's correspond remarkably well with the calculated FS's labeled (2) and (3), which are primarily associated with the plane bands.[12–15]

In our data there is not clear indication of the small FS pocket near the $\bar{S}$ point [labeled (4) in Fig. 3]. The EDC's for **k** near the **S** point are essentially featureless (Fig. 2). We note, however, that spectral intensities can have a strong dependence on photon energy and polarization and can vary between the first and higher BZ's. These measurements (Fig. 2) were made using $h\nu=21.2$ eV with photon polarization parallel to the crystallographic $a(b)$ axis. Recent measurements (with the same configuration of photon polarization and sample orientation), varying the photon energy in both the low-energy range (15–30 eV) (Ref. 37) and high-energy range (50–80 eV) (Ref. 38), also fail to show spectral features that would indicate a Fermi-level crossing in the vicinity of the $\bar{S}$ point in the first BZ. An early ARPES study[4] reported the observation of this piece of the FS using $h\nu=50$ eV. de Haas–van Alphen experiments[10,11] also reported observing this piece of the FS. Also, in the $h\nu=21.2$ eV data (Figs. 1 and 2), there is no clear evi-

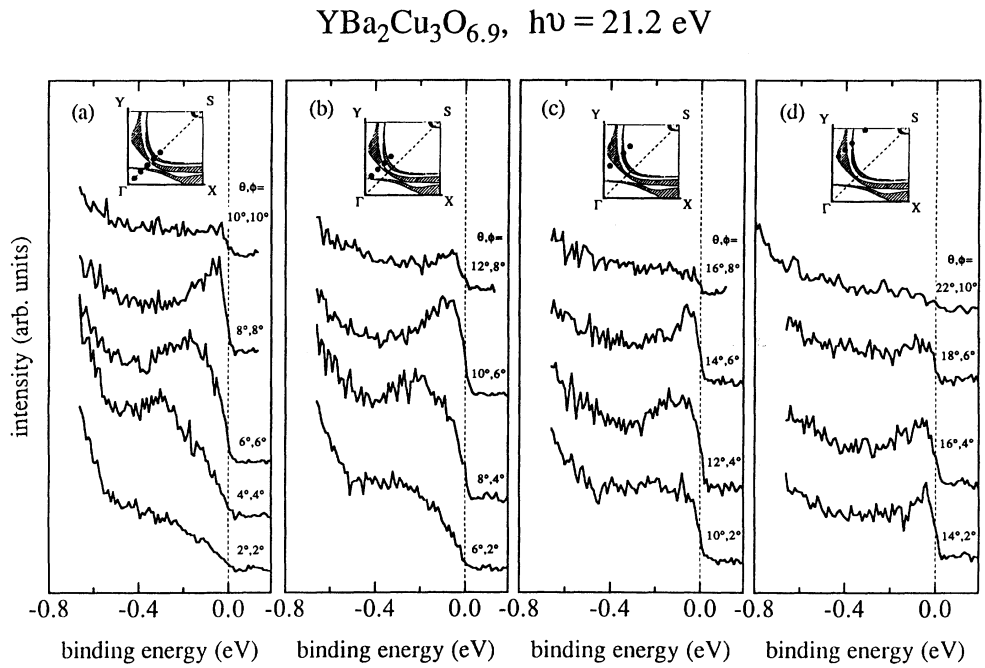

FIG. 4. EDC's measured on a $x=6.9$ sample, for **k** points (a) along the $\bar{\Gamma}$-$\bar{S}$ line and (b)–(d) along lines parallel to $\bar{\Gamma}$-$\bar{S}$. **k** points corresponding to the displayed EDC's appear as solid circles in the insets.

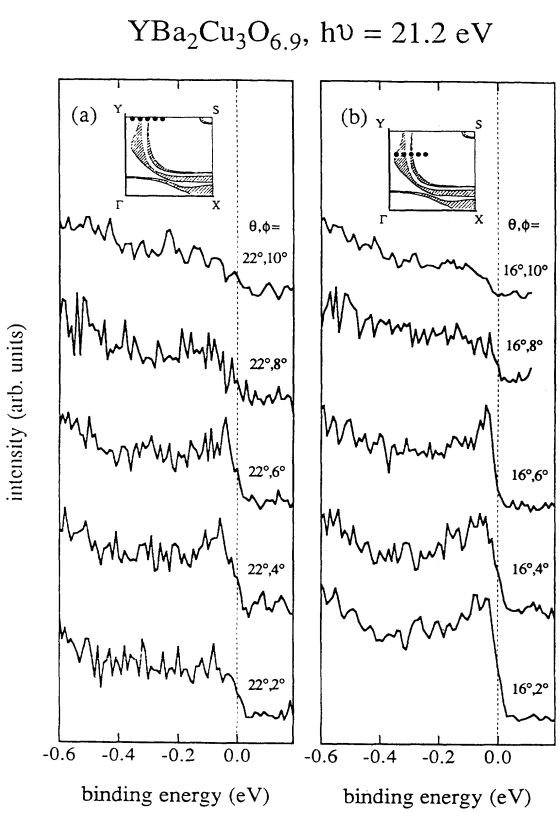

FIG. 5. EDC's measured on a $x=6.9$ sample, for **k** points along lines parallel to $\bar{\Gamma}$-$\bar{Y}(\bar{X})$ when the θ angle was held at (a) $\theta=22°$ and (b) $\theta=16°$. **k** points corresponding to the displayed EDC's appear as solid circles in the insets.

dence for the chain-related FS labeled (1) in the region near the $\bar{\Gamma}$ point. Observation of this FS was reported in positron-annihilation experiments.[8,9]

The spectral behavior and FS's near the $\bar{X}(\bar{Y})$ point are complex. It was shown by Tobin *et al.*[6] that the appearance of spectral features in EDC's for **k** points in that region of the BZ depends strongly on photon energy. Extraordinarily narrow and intense peaks were observed very close to E_F near the $\bar{Y}$ point when using $h\nu=17$ and 28 eV. The strong spectral dependence on photon energy may be a result of different values of matrix elements for transitions to different final states or non-negligible k_z dispersion, since the value of k_z is changed when the photon energy is varied. The relatively wide shaded region of the projected FS near the $\bar{X}$ point indicates that significant k_z dispersion is expected near $\bar{X}$. The dependence of these intense features on oxygen stoichiometry will be discussed in the later sections.

We note that the observed FS's also have reasonable correspondence with the FS's predicted by Abrikosov and Falkovsky[19] using a model, considering a single CuO_2 plane, where electrons belong to two groups: (1) $3d$ electrons localized on Cu atoms with single occupation (one hole per Cu atom) because of the large Coulomb interaction and (2) conduction electrons in bands formed by oxygen $2p$ states. The correspondence between theory and experiment is particularly good for intermediate levels of doping (middle panel of Fig. 4 in Ref. 19).

By monitoring spectral features in the vicinity of a Fermi-level crossing at temperatures at 20 K (well below T_c) and above T_c, we sought (unsuccessfully) to observe and measure the superconducting gap.[27] Possible reasons

for not being able to see a gap by photoemission were discussed at length by Tobin *et al.*[6] We note, however, that Ratz *et al.*[39] have recently reported observation of the superconducting gap in $YBa_2Cu_3O_x$ $(6.8<x<6.9)$ at a Fermi-level crossing along $\bar{\Gamma}$-$\bar{X}(\bar{Y})$. The authors correlate the behavior of a pronounced 1-eV peak near the $\bar{X}(\bar{Y})$ point with the presence or absence of a gap. Their data were taken using 18-eV incident photons. They report that an apparent gap appears only when the 1-eV peak is zero or heavily attenuated (a sample-dependent phenomenon). Variations of the 1-eV peak and structure near E_F are attributed to different surface terminations that are obtained when samples are cleaved. In our experiments we have extensively monitored the 1-eV peak using 24-eV photons; at this energy, the peak appears with much greater intensity than at 18 eV. In our samples the 1-eV peak is essentially always present, with high intensity, after a fresh *in situ* cleave. For different cleaves relative intensities of chemically shifted Ba 4*d* core levels are seen to vary dramatically; this is often interpreted to mean that different combination of terminations exist on the cleaved surfaces.[37] Yet the different exposed surfaces do not affect the presence or magnitude of the 1-eV peak. On the other hand, as samples "age" after many hours in the vacuum system, the intensity of the 1-eV peak becomes substantially reduced. Furthermore, the peak is dramatically attenuated when the samples become sufficiently oxygen deficient to show semiconducting behavior (see Sec. III C and Fig. 11). In our judgement the loss of this peak is an indication of a degraded sample surface. If this conclusion is correct, then the apparent observation of a gap by Ratz *et al.* may be a manifestation of an unsatisfactory sample surface (e.g., perhaps an insulating layer).

B. $YBa_2Cu_3O_{6.5}$

In $YBa_2Cu_3O_{6.5}$, one-half of the oxygen sites in the chain basal plane are vacant. It is known that the oxygen vacancies have a strong tendency to order into alternately filled and empty chains to form the ortho II structure.[22–24] Furthermore, the state of order has a strong effect on the superconducting properties.[25] The oxygens in the chain basal plane are sufficiently mobile so that ordering can occur slowly at room temperature after reduced stoichiometries are established by quenching.

Before photoemission measurements were taken, crystals were maintained at room temperature for more than 2 weeks after quenching, long enough for the samples to achieve a stable superconducting transition temperature. Shown in Fig. 6 are EDC's measured on a $x=6.5$ ($T_c=50$ K, twinned) sample, for **k** points along (a) a line 45° from $\bar{\Gamma}$-$\bar{Y}(\bar{X})$ (corresponding to $\bar{\Gamma}$-$\bar{S}$ in the BZ of $YBa_2Cu_3O_7$) and (b) $\bar{\Gamma}$-$\bar{Y}(\bar{X})$. This is essentially the same set of **k** vectors as those shown in Fig. 1 for a $x=6.9$ sample. Comparing Figs. 1 and 6, we observe that, along $\bar{\Gamma}$-$\bar{S}$, dispersing features appear with comparable spectral weight and cross the Fermi level at about the same **k** points for the two stoichiometries. Along $\bar{\Gamma}$-$\bar{Y}(\bar{X})$, the EDC's for $x=6.5$ show a feature near E_F with dispersing behavior resembling that of $x=6.9$. However, for the

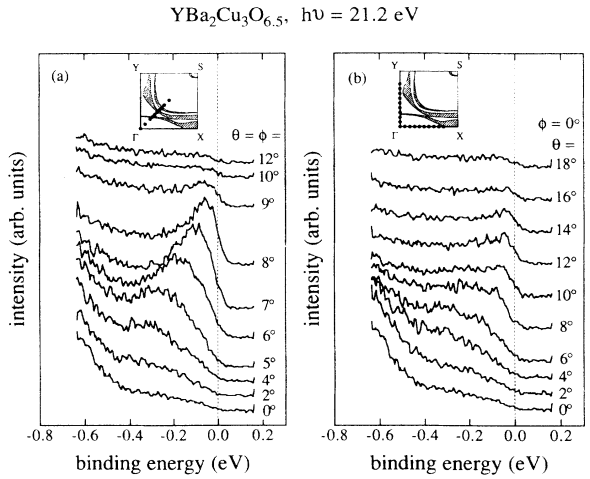

FIG. 6. EDC's measured on a $x=6.5$ sample using $h\nu=21.2$ eV, for **k** points along the (a) $\bar{\Gamma}$-$\bar{S}$ and (b) $\bar{\Gamma}$-$\bar{Y}(\bar{X})$ symmetry directions of the Brillouin zone (for $YBa_2Cu_3O_7$). This is the same set of measurements shown in Fig. 1 for a $x=6.9$ sample.

$x=6.9$ sample, a clear Fermi-level crossing is indicated by the sudden drop of intensity for $\theta>15°$; for the $x=6.5$ sample, it is not apparent that the dispersing band crosses E_F. The band may only approach E_F with maximum intensity near $\theta=12°$. Further, the spectral weight of the peak is significantly less for the $x=6.5$ sample.[28]

Shown in Fig. 7 are EDC's taken from a $x=6.5$ sample, using $h\nu=21.2$ eV, when **k** was scanned on a grid of points in **k** space; the display format is the same as that of Fig. 2. It is evident that the spectral intensity variation and dispersing behavior throughout the BZ are strikingly similar for $x=6.5$ and 6.9 stoichiometries. In general, a strong resemblance in the spectral line shapes can be observed in the EDC's for the two stoichiometries at equivalent **k** points. When differences occur, they tend to be rather subtle, as illustrated above in the comparison between Figs. 1 and 6. We observe, for example, that corresponding EDC's in columns 2 ($\phi=4°$, Figs. 2 and 7) have comparable spectral intensities, line shapes, and dispersive character, whereas corresponding EDC's in columns 1 ($\phi=2°$) appear with less intensity when $x=6.5$ than when $x=6.9$. Particularly noticeable differences occur at ($\theta=16°$, $\phi=2°$) and ($\theta=12°$, $\phi=2°$); Fermi-level crossings are not apparent at these angles when $x=6.5$.

Extraordinarily narrow features were observed near E_F in untwinned $x=6.9$ samples using $h\nu=17$ and 28 eV.[6] Remarkably, those features are also observed, with comparable width and intensity, in an untwinned $x=6.5$ sample. Shown in Fig. 8 are EDC's measured on an untwinned $x=6.5$ sample ($T_c=53$ K) for **k** points along the $\bar{\Gamma}$-$\bar{Y}$-$\bar{\Gamma}'$ line using $h\nu=28$ eV. In going from $\bar{\Gamma}$ to the $\bar{Y}$ point, a peak is seen to disperse toward E_F. The peak stays at E_F for a number of **k** points along the $\bar{\Gamma}$-$\bar{Y}$-$\bar{\Gamma}'$ line (from $\theta=12°$ to 28°) and then disperses back to higher binding energy as the $\bar{\Gamma}'$ point is approached, as expected from crystal symmetry.

Shown in Fig. 9 are EDC's measured on an untwinned

$x=6.5$ sample for **k** points near the $\bar{Y}$ point using $h\nu=17$ eV. Again, a very narrow peak, which persists at E_F for a number of **k** points, can be observed. The width of this peak is comparable to the instrument resolution. A nearly identical feature was observed on untwinned $x=6.9$ samples by Tobin *et al.*[6]

To summarize these observations, most of the spectral features near E_F are found to be unchanged, within resolution limitations, as the oxygen stoichiometry is reduced from $x=6.9$ to 6.5. Stable spectral features include the unusually sharp peaks near the $\bar{Y}$ point observed when using $h\nu=28$ and 17 eV. Most of the points on the two large FS's, formed from plane-related bands, also show no discernible change with oxygen variation.

However, significant spectral changes were observed, as x was varied, when **k** was in a region near the $\bar{\Gamma}$-$\bar{Y}$($\bar{X}$) line (with $h\nu=21.2$ eV). The features appear with less intensity at $x=6.5$ than at $x=6.9$. Also, Fermi-level crossings appear to be somewhat shifted in the BZ. Since the data were taken on twinned samples, the observed changes could be associated with features appearing along either the $\bar{\Gamma}$-$\bar{Y}$ or $\bar{\Gamma}$-$\bar{X}$ line. If these features occur near $\bar{\Gamma}$-$\bar{Y}$, comparison to Fig. 3 suggests that, at $x=6.5$, the FS size is somewhat reduced in the vicinity of the bulge area near $\theta=14°$, i.e., in the outer plane-related FS. Also, some calculations (e.g., Ref. 12) show a chain-related band crossing E_F along Γ-Y. Thus the observed spectral changes with reduced oxygen stoichiometry could also be associated with loss of this chain-related FS. On the other hand, if these stoichiometry dependent features occur near $\bar{\Gamma}$-$\bar{X}$, then they must be associated with "ridge" FS [labeled (1) in Fig. 3]. Measurements on untwinned crystals are needed to further clarify these issues.

It is generally recognized that the oxygen content in $YBa_2Cu_3O_x$ controls the carrier concentration.[26,40] It is not clear, however, how the hole concentration varies in the planes and chains respectively, as the oxygen content is varied, although bond-valence-sum analyses provide semiquantitative information.[41,42] According to Luttinger's theorem, changes in carrier concentration should be reflected in the size of the FS cross-sectional areas (for a two-dimensional material), and in principle, plane and chain variations should be separately observable. Most of the Fermi-level crossings were found to be invariant as oxygen content was reduced from $x=6.9$ to 6.5. However, as discussed above, the size of the outer plane-related FS near $\bar{\Gamma}$-$\bar{Y}$ might be somewhat reduced as oxygen is depleted, signaling the expected reduction in hole concentration. If, however, the observed $\bar{\Gamma}$-$\bar{Y}$($\bar{X}$)

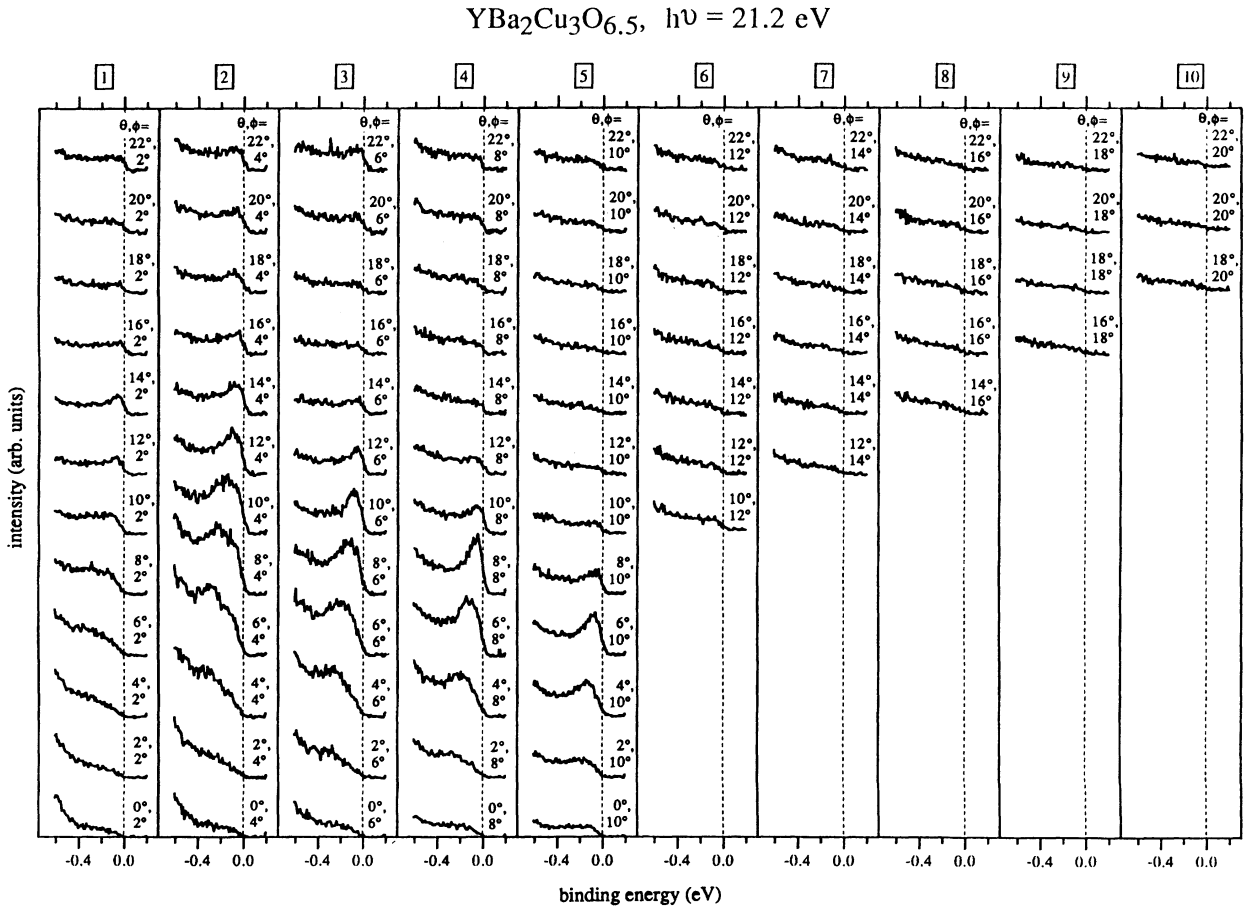

FIG. 7. EDC's measured on a $x=6.5$ sample using $h\nu=21.2$ eV. The display format is the same as that of Fig. 2.

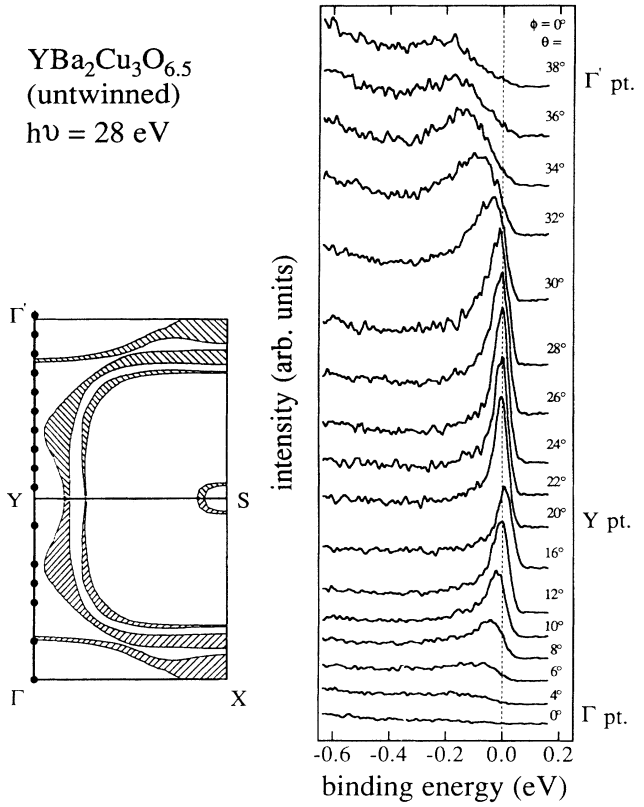

FIG. 8. EDC's measured on an untwinned $x=6.5$ sample ($T_c=53$ K), for **k** points along the $\bar{\Gamma}$-$\bar{Y}$-$\bar{\Gamma}'$ line, using $h\nu=28$ eV.

spectral variations are found to occur near the $\bar{\Gamma}$-$\bar{X}$ line, then band theory (Fig. 3) suggests that carrier-concentration changes, with varied x, primarily occur in the "ridge" FS.

These measurements do not provide a good quantitative measure of carrier-concentration changes. Considering the **k** resolution of these ARPES experiments ($|\Delta\mathbf{k}|=0.075$ Å^{-1}, at $h\nu=21.2$ eV) and the comparable separation of **k** points between measured EDC's, the uncertainty in our measurements of the large plane-related FS areas could be as large as 20%.

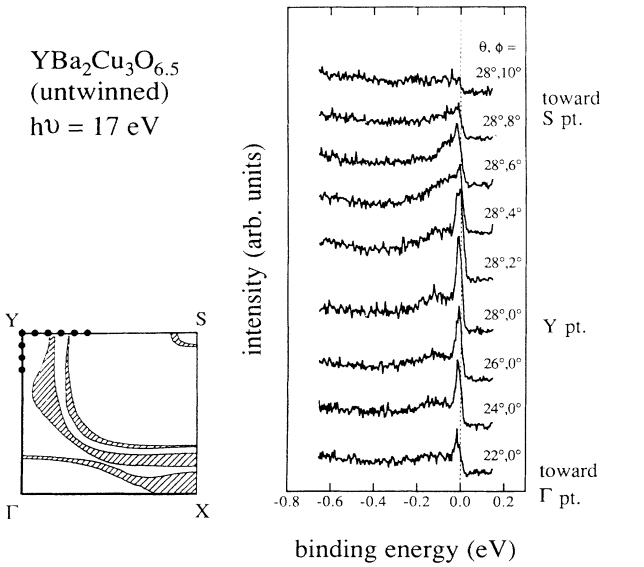

FIG. 9. EDC's measured on an untwinned $x=6.5$ sample, for **k** points near the $\bar{Y}$ point, using $h\nu=17$ eV.

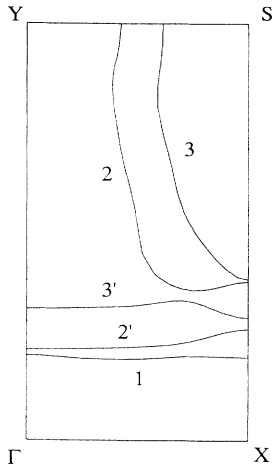

FIG. 10. Fermi surfaces of $YBa_2Cu_3O_{6.5}$ calculated by Yu *et al.* (Ref. 43) for the double-cell ortho II structure.

The electronic structure for $YBa_2Cu_3O_{6.5}$ was calculated for the double-cell ortho II structure by Yu *et al.*[43] using the LDA approach. The FS's are shown in Fig. 10. At $x=6.5$, cell doubling along the a axis halves the BZ along the $\bar{\Gamma}$-$\bar{X}$ direction. We observe in Fig. 10 that the plane-related FS's [labeled (2), (3), (2'), and (3')] are very similar to those of $YBa_2Cu_3O_7$ (Fig. 3) except for a doubling of the number of plane bands (a folding of the plane bands from the BZ of $YBa_2Cu_3O_7$) and some modifications near the new zone boundary. The chain-related FS [labeled (1)] is also very similar to the corresponding FS in Fig. 3 (but this band is not doubled in the new zone). The observed spectral similarities between $x=6.5$ and 6.9 are consistent with these predictions.

While it is recognized that LDA calculations on $YBa_2Cu_3O_6$ are incorrect (they predict metallic behavior, whereas the material is insulating), we note that such calculations show that all chain bands are missing, but the plane bands are relatively unchanged compared with band structure of $YBa_2Cu_3O_7$.[12,15,44] These band-calculation results suggest a general trend; that is, as oxygen is depleted from $YBa_2Cu_3O_7$, chain bands are systematically lost, while plane bands remain relatively unchanged.

C. $YBa_2Cu_3O_{6.3-6.35}$

Several samples with oxygen stoichiometry x being approximately 6.3–6.35 were studied. These samples are not superconducting, but the stoichiometries are very close to the metal-insulator transition. The structures are slightly orthorhombic.[25] Resistivity measurements (taken on some of these samples) show semiconducting behavior with an increasing resistivity for decreasing temperature

below about 70 K (see Fig. 3 of Ref. 28).

As shown above, relatively small spectral variation was observed between samples of different oxygen content when the stoichiometry was varied in the metallic region. However, very distinct spectral changes are apparent when the sample becomes insulating.[28] Figure 11 compares EDC's taken from a $x=6.35$ sample (dashed lines) and from a $x=6.9$ sample (solid lines), for several **k** points along the $\bar{\Gamma}$-$\bar{Y}(\bar{X})$ line, using $h\nu=17$ eV. It is clear that the sharp and intense feature near E_F, apparent when $x=6.9$, disappears in the nonsuperconducting $x=6.35$ sample. Shown in Fig. 12 are EDC's taken from a $x=6.3$ sample using $h\nu=28$ eV for **k** points along the $\bar{\Gamma}$-$\bar{Y}(\bar{X})$-$\bar{\Gamma}'$ line, with the same increment between **k** points as shown in Fig. 8 for an untwinned $x=6.5$ sample. Obviously, the intense peak near E_F, apparent when $x=6.5$, is absent when $x=6.3$, although a residual of the underlying band dispersion is visible. The underlying structure is similar to that observed along $\bar{\Gamma}$-$\bar{X}$-$\bar{\Gamma}'$ on untwinned $x=6.9$ samples.[37] This suggests that it could be of CuO_2 plane origin, since the plane structure has fourfold symmetry and is relatively unchanged when oxygen content is reduced.

Shown in Fig. 13(a) are EDC's taken on a $x=6.3$ sample, for **k** points along $\bar{\Gamma}$-$\bar{S}$, using $h\nu=21.2$ eV. We observe that significantly reduced spectral weight occurs near E_F in these data relative to those for $x=6.9$ and 6.5 [compare Figs. 1(a) and 6(a); also see Ref. 28]. Nonetheless, the spectral features continue to show dispersion, even suggesting a Fermi-level crossing near $\theta=\phi=9°$. No effect of an insulating gap was observed, perhaps because the gap is much smaller than the instrument resolution function.

Shown in Figs. 13(b) and 13(c) are EDC's taken on a $x=6.3$ sample, for **k** points along lines parallel to $\bar{\Gamma}$-$\bar{S}$ (solid circles in the insets). As the lines become more remote from $\bar{\Gamma}$-$\bar{S}$, dispersion becomes much less apparent and Fermi-level crossings are not observed [Fig. 13(c)]. Presumably, the apparent Fermi-level crossings seen in Fig. 13(a) [and, perhaps, in Fig. 13(b)] are the residual of a FS (i.e., bands dispersing toward E_F but separated from the Fermi level by a small gap). These results indicate that, near the metal-insulator transition, the FS only exists in a small region of the BZ. This contrasts with the large FS's seen in $x=6.9$ and 6.5 samples; Fig. 4 shows that Fermi-level crossings are clearly seen in regions far away from $\bar{\Gamma}$-$\bar{S}$ in $x=6.9$ samples.

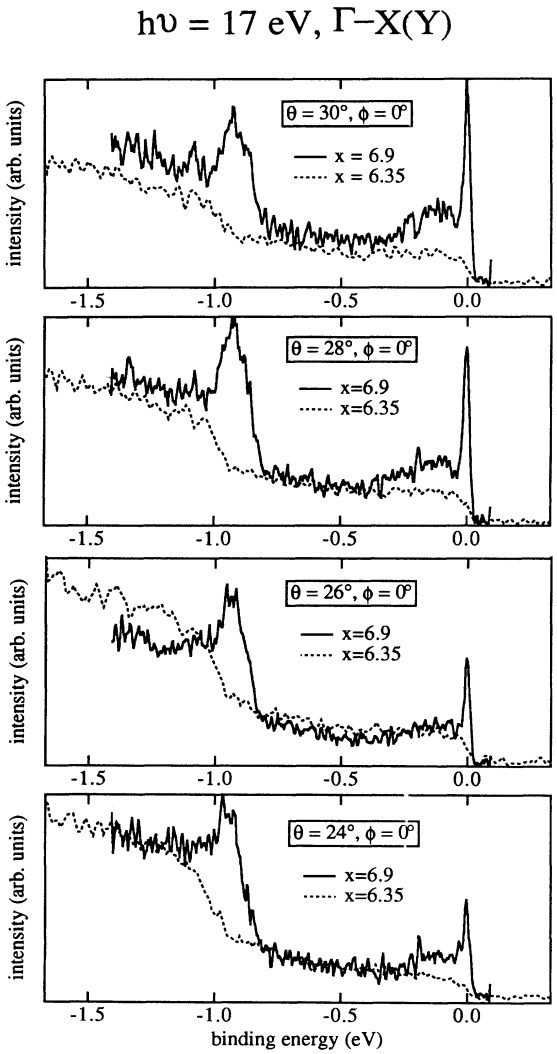

FIG. 11. Comparison of the EDC's measured on a $x=6.35$ sample (dashed lines) and a $x=6.9$ sample (solid lines), for several **k** points on the $\bar{\Gamma}$-$\bar{Y}(\bar{X})$ line, using $h\nu=17$ eV.

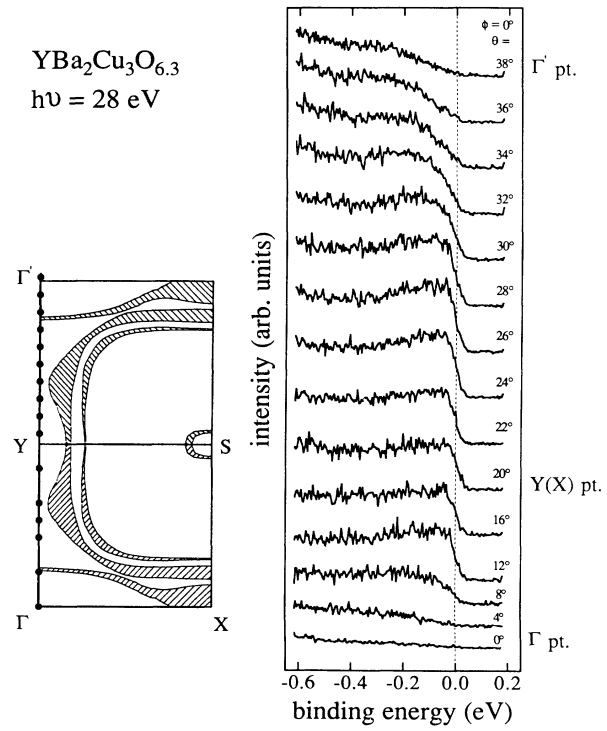

FIG. 12. EDC's measured on a $x=6.3$ sample, for **k** points along the $\bar{\Gamma}$-$\bar{Y}(\bar{x})$-$\bar{\Gamma}'$ line, using $h\nu=28$ eV. This is the same set of measurements shown in Fig. 8 for a $x=6.5$ sample.

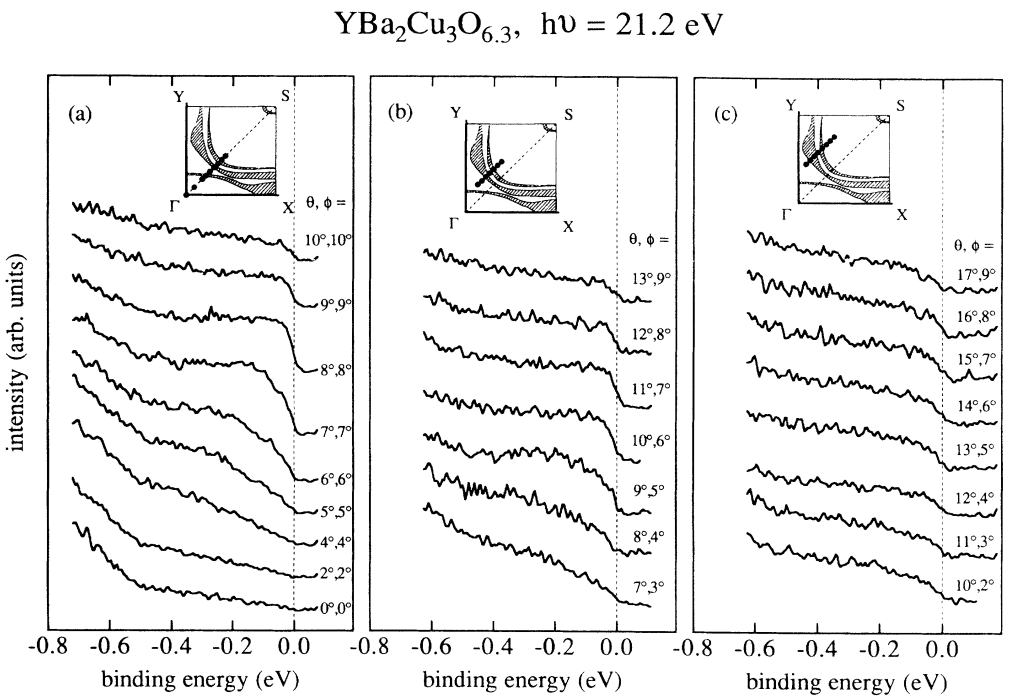

FIG. 13. EDC's measured on a $x = 6.3$ sample, for **k** points (a) along the $\bar{\Gamma}$-$\bar{S}$ line and (b) and (c) along lines parallel to $\bar{\Gamma}$-$\bar{S}$. **k** points corresponding to the displayed EDC's appear as solid circles in the insets.

Some model theories[19,45] predict small FS's, as illustrated in Fig. 14 (taken from Ref. 19), for stoichiometries near the metal-insulator transition where doping level are low. The spectra of Fig. 13 provide some support for this picture, since bands dispersing through E_F are only observed close to the zone diagonal $\bar{\Gamma}$-$\bar{S}$. However, to form such a closed FS, one expects to see, from $\bar{\Gamma}$ to $\bar{S}$, a band that first disperses from below E_F to above E_F and then disperses back from above E_F to below E_F. In other words, after the occurrence of the first Fermi-level crossing, the EDC's should show the occurrence of a reentrant spectral peak, resulting from a band dispersing from above E_F to below E_F, as **k** exceeds the second Fermi-level crossing. In an effort to observe the band reentrant behavior, we measured EDC's with an angular increment of 1° or 2° from the $\bar{\Gamma}$ point all the way to the $\bar{S}$ point, for oxygen stoichiometries $x = 6.35$, 6.4, 6.5, 6.7, and 6.9.

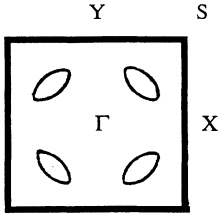

FIG. 14. Schematic Fermi surfaces suggested by some model theories (Refs. 19 and 44) for stoichiometries near the metal-insulator transition where hole-doping levels are low.

The spectra of $x = 6.35$ and 6.5 are shown in Fig. 15. Note that, for both stoichiometries, after the bands first cross E_F at about $\theta = \phi = 9°$, the spectral intensity becomes very low and remains very low all the way to $\theta = \phi = 24°$ (near the $\bar{S}$ point). The expected band reentrance is apparently not observed. Measurements for other oxygen stoichiometries show similar results. For a $x = 6.35$ sample, some measurements were also made using different photon energies in the range 15–28 eV. No evidence of band reentrance was observed under these measurement conditions either.

Results such as those in Fig. 15(b) can also provide an additional test of band-theory predictions for the $x = 6.5$ ortho II structure. The BZ edge along $\bar{\Gamma}$-$\bar{X}$ for $x = 6.5$ is about half of the $\bar{\Gamma}$-$\bar{X}$ distance for $x = 7$; a new periodicity occurs. Band reentrant behavior should appear in the second zone of the new cell [reflection symmetry occurs about the $\bar{X}$-$\bar{S}$ line (Fig. 10)] when **k** is scanned along the line 45° from $\bar{\Gamma}$-$\bar{X}$ (i.e., $\theta = \phi$). As seen in Fig. 15(b), there is no indication in the spectra for the new periodicity; i.e., the spectra do not show symmetry with respect to the new zone boundary. It may be that the states being probed (primarily plane related) are not dramatically perturbed by the new periodicity, so that the effect of cell doubling cannot be observed at this level of sensitivity.

IV. SUMMARY

An extensive set of ARPES measurements was made on $YBa_2Cu_3O_x$ crystals with oxygen stoichiometries $x = 6.9$, 6.5, and 6.3, which include, respectively, a 92-K

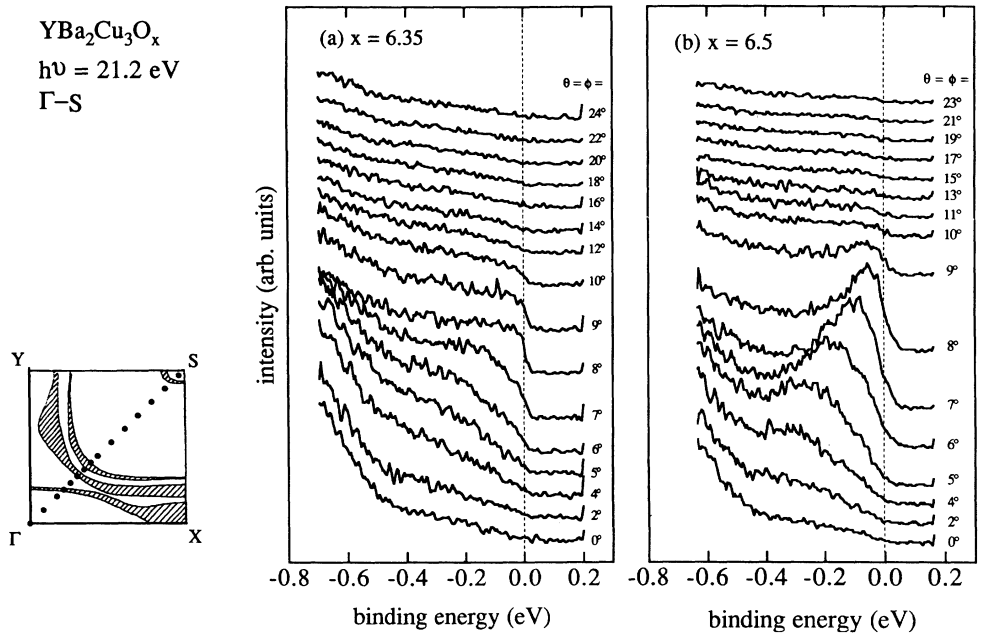

FIG. 15. EDC's measured on (a) $x = 6.35$ and (b) $x = 6.5$ samples, with **k** scanning from $\bar{\Gamma}$ to S.

superconductor in the ortho I structure, an approximately 50-K superconductor in the ortho II structure, and an insulating sample with stoichiometry very close to the metal-insulator transition. Spectral behavior near E_F was examined throughout the first Brillouin zone. By observing the dispersion of spectral features as a function of **k** and determining the **k** points at which peaks disperse across E_F, Fermi surfaces were measured.

For $x = 6.9$, two large FS's were observed. They have remarkably good correspondence with the two plane-related FS's predicted by LDA calculations. Most of the chain-related FS's predicted by LDA calculations were not clearly identified in the data.

For $x = 6.5$, the spectral behavior throughout the BZ was observed to be strikingly similar to that of $x = 6.9$. In particular, for the plane-related features, the spectra taken at equivalent **k** points are very similar for the two stoichiometries. The most discernible change are observed in EDC's, from twinned crystals, taken along the BZ edge, $\bar{\Gamma}$-$\bar{Y}$($\bar{X}$). In those EDC's, a substantial reduction in spectral intensity was observed for $x = 6.5$ relative to $x = 6.9$. Small changes in FS dimensions may also be observable. Since twinned samples were measured, it cannot be determined if the changes are more likely to be associated with a reduction in the size of a plane-related FS near $\bar{\Gamma}$-$\bar{Y}$ or if the changes are associated with the "ridge" FS along $\bar{\Gamma}$-$\bar{X}$. Data from twin-free crystals are required in order to resolve this issue.

For $x = 6.3$, significant spectral changes occur. Notably, sharp and intense features near E_F, observed at $x = 6.9$ and 6.5, disappear or severely broaden at $x \approx 6.3$. These results strongly suggest that the electron states that produce these sharp features must exert an important influence on the transport properties.

In the insulating $x \approx 6.3$ material, spectral features dispersing through E_F were observed along some directions of the BZ, suggesting (within resolution limitations) an apparent FS. However, these apparent crossings were only observed in a small region of the BZ, indicating a small FS. This is in contrast with the large FS's observed in the $x = 6.9$ and 6.5 samples. Apparently, the reduced FS dimensions and the loss of sharp features near E_F are indications of the onset of strong correlation effects responsible for the insulator behavior.

ACKNOWLEDGMENTS

The authors gratefully acknowledge Dr. J. J. Yu and Professor A. J. Freeman for permission to use their results for the ortho II structure prior to publication. Work at Argonne National Laboratory is supported by the U.S. DOE under Contract No. W-31-109-ENG-38 (B.W.V., A.P.P., J.W.D., P.J.K., and S.F.) and by the NSF, Science and Technology Center for Superconductivity, under Contract No. DMR 8809854 (R.L. and U.W.). Ames Laboratory is operated for the U.S. DOE by Iowa State University under Contract No. W-7405-ENG-82. The Synchrotron Radiation Center is supported by the NSF under Contract No. DMR 8601349.

[1]For a review, see K. Levin, J. H. Kim, J. P. Lu, and Q. Si, Physica C **175**, 449 (1991); in *Physical Properties of High Temperature Superconductors I*, edited by Donald M. Ginsberg (World Scientific, Singapore, 1989).

[2]C. G. Olson, R. Liu, D. W. Lynch, R. S. List, A. J. Arko, B. W. Veal, Y. C. Chang, P. Z. Jiang, and A. P. Paulikas, Phys. Rev. B **42**, 381 (1990).

[3]G. Mante, R. Claessen, T. Buslaps, S. Harm, R. Manzke, M.

Skibowski, and J. Fink, Z. Phys. B **80**, 181 (1990).
[4]J. C. Campuzano, G. Jennings, M. Faiz, L. Beaulaigue, B. W. Veal, J. Z. Liu, A. P. Paulikas, K. Vandervoort, H. Claus, R. S. List, A. J. Arko, and R. J. Bartlett, Phys. Rev. Lett. **64**, 2308 (1990).
[5]J. C. Campuzano, G. Jennings, A. J. Arko, R. S. List, B. W. Veal, and R. Benedek, J. Phys. Chem. Solids. **52**, 1411 (1991).
[6]J. G. Tobin, C. G. Olson, C. Gu, J. Z. Liu, F. R. Solal, M. J. Fluss, R. H. Howell, J. C. O'Brien, H. B. Radousky, and P. A. Sterne, Phys. Rev. B **45**, 5563 (1992).
[7]G. Mante, R. Claessen, A. Hub, R. Manzke, M. Skibowski, Th. Wolf, M. Knupfer, and J. Fink, Phys. Rev. B **44**, 9500 (1991).
[8]L. C. Smedskjaer, J. Z. Liu, R. Benedek, D. G. Legnini, D. J. Lam, M. D. Stahulak, H. Claus, and A. Bansil, Physica C **156**, 269 (1988).
[9]H. Haghighi, J. H. Kaiser, S. Raynder, R. N. West, J. Z. Liu, R. Shelton, R. Howell, F. Solal, and M. J. Fluss, Phys. Rev. Lett. **67**, 382 (1991).
[10]F. M. Mueller, C. M. Fowler, B. L. Freeman, W. L. Hults, J. C. King, and J. L. Smith, Physica B **172**, 253 (1991).
[11]G. Kido, K. Komorita, H. Katayama-Yoshida, and T. Takahashi, J. Phys. Chem. Solids **52**, 1465 (1991).
[12]J. Yu, S. Massidda, A. J. Freeman, and D. D. Koelling, Phys. Lett. A **122**, 203 (1987); A. J. Freeman, J. Yu, S. Massidda, and D. D. Koelling, Physica B **148**, 212 (1987).
[13]H. Krakauer, W. E. Pickett, and R. E. Cohen, J. Superconductivity **1**, 111 (1988).
[14]W. E. Pickett, Rev. Mod. Phys. **61**, 433 (1989).
[15]W. E. Pickett, R. E. Cohen, and H. Krakauer, Phys. Rev. B **42**, 8764 (1990).
[16]P. W. Anderson, Phys. Rev. B **42**, 2624 (1990); Phys. Rev. Lett. **64**, 1839 (1990).
[17]P. A. Lee, Phys. Rev. Lett. **63**, 680 (1989); N. Nagaosa and P. A. Lee, *ibid.* **64**, 2450 (1990).
[18]C. M. Varma, P. B. Littlewood, S. Schmitt-Rink, E. Abrahams, and A. E. Ruckenstein, Phys. Rev. Lett. **63**, 1996 (1989).
[19]A. A. Abrikosov and L. A. Falkovsky, Physcia C **168**, 556 (1990).
[20]P. W. Anderson and J. R. Schrieffer, Phys. Today **44** (6), 55 (1991).
[21]J. D. Jorgensen, B. W. Veal, A. P. Paulikas, L. J. Nowicki, G. W. Crabtree, H. Claus, and W. K. Kwok, Phys. Rev. B **41**, 1864 (1990).
[22]J. Reyes-Gasga, T. Krekels, G. Van Tendeloo, J. Van Landuyt, S. Amelinckx, W. H. M. Briggink, and H. Verweij, Physica C **159**, 831 (1989).
[23]M. Hervieu, B. Domengès, B. Raveau, M. Post, W. R. McKinnon, and J. M. Tarascon, Mater. Lett. **8**, 73 (1989).
[24]D. deFontaine, G. Ceder, and M. Asta, J. Less-Common Met. **164&165**, 108 (1990); Nature **343**, 544 (1990).
[25]B. W. Veal, A. P. Paulikas, Hoydoo You, Hao Shi, Y. Fang, and J. W. Downey, Phys. Rev. B **42**, 4770 (1990); **42**, 6305 (1990); J. D. Jorgensen, S. Pei, P. Lightfoot, H. Shi, A. P. Paulikas, and B. W. Veal, Physica C **167**, 571 (1990); H. Claus, S. Yang, A. P. Paulikas, J. W. Downey, and B. W. Veal, *ibid.* **171**, 205 (1990).
[26]B. W. Veal and A. P. Paulikas, Physica C **184**, 321 (1991).
[27]R. Liu, B. W. Veal, A. P. Paulikas, J. W. Downey, H. Shi, C. G. Olson, C. Gu, A. J. Arko, and J. J. Joyce, J. Phys. Chem. Solids **52**, 1437 (1991).
[28]R. Liu, B. W. Veal, A. P. Paulikas, J. W. Downey, H. Shi, C. G. Olson, C. Gu, A. J. Arko, and J. J. Joyce, Phys. Rev. B **45**, 5614 (1992).
[29]D. L. Kaiser, F. Holtzberg, B. A. Scott, and T. R. McGuire, Appl. Phys. Lett. **51**, 1040 (1987); L. F. Schneemeyer, J. V. Waszczak, T. Siegrist, R. B. van Dover, L. W. Rupp, B. Batlogg, R. J. Cava, and D. W. Murphy, Nature **328**, 601 (1987); J. P. Rice, B. G. Pazol, D. M. Ginsberg, T. J. Moran, and M. B. Weissman, J. Low. Temp. Phys. **72**, 345 (1988).
[30]K. G. Vandervoort, G. Griffith, H. Claus, and G. W. Crabtree, Rev. Sci. Instrum. **62**, 2271 (1991).
[31]U. Welp, M. Grimsditch, H. You, W. K. Kwok, M. M. Fang, G. W. Crabtree, and J. Z. Liu, Physica C **161**, 1 (1989).
[32]C. G. Olson, Nucl. Instrum. Methods A **266**, 205 (1988).
[33]A. J. Arko, R. S. List, R. J. Barlett, S. W. Cheong, Z. Fisk, J. D. Thompson, C. G. Olson, A. B. Yang, R. Liu, C. Gu, B. W. Veal, J. Z. Liu, A. P. Paulikas, K. Vandervoort, H. Claus, J. C. Campuzano, J. E. Schirber, and N. D. Shinn, Phys. Rev. B **40**, 2268 (1989).
[34]C. G. Olson, R. Liu, A.-B. Yang, D. W. Lynch. A. J. Arko, R. S. List, B. W. Veal, Y. C. Chang, P. Z. Jiang, and A. P. Paulikas, Science **245**, 731 (1989).
[35]R. Manzke, T. Buslaps, R. Claessen, and J. Fink, Europhys. Lett. **9**, 477 (1989).
[36]J.-M. Imer, F. Pathey, B. Dardel, W.-D. Schneider, Y. Baer, Y. Petroff, and A. Zettl, Phys. Rev. Lett. **62**, 336 (1989).
[37]C. G. Olson *et al.* (unpublished); also see R. Liu *et al.*, Phys. Rev. B **40**, 2650 (1989).
[38]R. Liu *et al.* (unpublished).
[39]S. Ratz, N. Schroeder, R. Böttner, E. Dietz, U. Gerhardt, and Th. Wolf, Solid State Commun. **82**, 245 (1992).
[40]M.-H. Whangbo and C. C. Torardi, Science **249**, 1143 (1990).
[41]R. J. Cava, A. W. Hewat, E. A. Hewat, B. Batlogg, M. Marezio, K. M. Rabe, J. J. Krajewski, W. F. Peck, Jr., and L. W. Rupp, Jr., Physica C **165**, 419 (1990).
[42]I. D. Brown, J. Solid State Chem. **82**, 122 (1989).
[43]J. Yu *et al.* (unpublished).
[44]F. Herman, R. V. Kasowski, and W. Y. Hsu, Phys. Rev. B **36**, 6904 (1987).
[45]P. A. Lee, in *High Temperature Superconductivity Proceedings,* edited by K. S. Bedell, D. Coffey, D. E. Meltzer, D. Pines, and J. R. Schrieffer (Addison-Wesley, Reading MA, 1990), p. 96.